Hybrid Conjugates Formed between Gold Nanoparticles and an Amyloidogenic Diphenylalanine-Cysteine Peptide

Juliane N. B. D. Pelin,[a] Dr. Emanuela Gatto,[b] Prof. Mariano Venanzi,[b] Dr. Francesca Cavalieri,[c] Dr. Cristiano L. P. Oliveira,[d] Dr. Herculano Martinho,[a] Dr. Emerson R. Silva,[e] Dr. Andrea M. Aguilar,[f] Dr. Juliana S. Souza,[a] Dr. Wendel A. Alves[a],*

[a]*Centro de Ciências Naturais e Humanas, Universidade Federal do ABC, 09210-580, Santo André, Brazil.*

[b]*Department of Chemical Science and Technologies, University of Rome Tor Vergata, Italy.*

[c]*Department of Chemical and Biomolecular Engineering, The University of Melbourne, Australia.*

[d]*Instituto de Física, Universidade de São Paulo, 05314-970, São Paulo, Brazil.*

[e]*Departamento de Biofísica, Universidade Federal de São Paulo, 04023-062, São Paulo, Brazil.*

[f]*Instituto de Ciências Ambientais, Químicas e Farmacêuticas, Universidade Federal de São Paulo, Diadema, 09972-270, Brazil.*

*Corresponding Author E-mail: wendel.alves@ufabc.edu.br. Tel.: +55 11 4996 0193. Fax: +55 11 4996 3166.

ABSTRACT

We investigated the effect of gold nanoparticles (AuNPs) on the aggregation of a CFF (C = cysteine; F = phenylalanine) tripeptide (derived from Aβ peptide) in aqueous medium. Special attention was dedicated to the role of AuNPs as inducers and inhibitors during nucleation kinetics and the structure of the resulting scaffolds was carefully investigated. At millimolar concentrations, the tripeptide was found to form β-sheet structures organized into long filaments. Spectral signatures and topography of the filaments were studied by Raman spectroscopy and atomic force microscopy (AFM), revealing that conjugation to AuNPs not only stabilizes the system, but also inhibit or enhance amyloid-like features depending on the synthesis route used in the preparation of AuNPs. Sodium borohydride ($NaBH_4$) mediated synthesis of AuNPs gave rise to a strong absorption peak close to 520 nm, indicating that AuNPs were dispersed, independently of the peptide concentration added in the reaction. However, when the peptide/gold salt mixture was heated at 60°C, AuNPs and AuNP-decorated filaments were both formed in solution and the fractions of which population were found to be dependent on the $[HAuCl_4]$/[CFF] ratio, as illustrated by TEM images. In addition, the insertion of AuNPs at the surface of CFF nanostructures can promote electron transfer from the metallic nanoparticles to the CFF surface, creating an *n*-type semiconductor, and causing a peak shift of the phenylalanine absorption band.

1. INTRODUCTION

The formation of metal nanoparticles decorated by short peptides is based on the reducing capability of metal ions and the capping ability of the peptides. Peptide sequence-activity relationships can be used to achieve shape and size control of the metal nanoparticles by varying the ratio of the metal ion to the peptide concentration.[1-4] Achieving control of such interactions is important for developing diagnostic and therapeutic strategies where protein and peptide aggregation is associated with disease.[5-12] Recent studies have shown that nanoparticles can have an impact on the aggregation properties of peptide or protein structures, where the cooperative binding of biomolecules to nanoparticles may be either beneficial or deleterious to the formation of amyloid structures.[13-18]

Interaction with nanoparticles may either affect the structure of amyloid-prone peptides, inducing the formation of β-structures that serve as nucleation centers for fibrillization, or bind intermediate units, and even temporary reverse the growth of fibrils or aggregate structures.[13,19-21] Identification of possible targets in the formation of amyloid structures is crucial for future application of nanotechnology to enhance specificity and efficacy of prevention and control methods of neurodegenerative diseases.

At the same time, amyloid-like peptide nanostructures (ALPNs) were shown to be able to control aggregation of metal nanoparticles into 1D nanostructures.[22,23] ALPNs can be specifically designed to have chemically active groups offering metal binding sites on their external surface. Previously, Schebeil *et al.*[24] applied layer by layer electrodeposition of Au and Ag on ALPNs, obtaining metal-peptide conjugates with conductive properties comparable to that of a solid metal wire.[24] In this connection, Chen and Rosi[25] reported that peptides can be used as scaffolds to control the nucleation and growth of inorganic materials.[25]

Diphenylalanine (FF) peptide, the core recognition motif of Alzheimer's β-amyloid polypeptide, is one of the most studied for the formation of self-organized structures.[26,27] The polymorphism of FF-based nanostructures can be controlled by the experimental incubation conditions such as solvent, peptide concentration, pH and temperature.[27-32] It has been shown that triphenylalanine peptides (FFF) self-assemble into nanospheres or nanorods, which are different from the nanovesicles and nanotubes formed by simply tuning the FF peptide concentration.[33-36]

In a pioneering study by Reches and Gazit,[26] it was found that FF self-assemblies serve as excellent sacrificial templates for fabrication of Ag nanowires through a reductive process.[26] Furthermore, a morphological transition was observed when phenylglycine (Phg) was used as the dipeptide motif.[37] Phg offers constrained rotational freedom around the C-C bond, which helps in the formation of very stable Phg-Phg nano vesicles. A similar morphological switch was also observed when FF dipeptide was conjugated to a cysteine residue (CFF).[38,39] This tripeptide self-assembled into soft nanospheres suggesting that the disulfide bridge formation results in the closure of nanotubes. However, a fine control of the CFF aggregation process has not yet been elucidated, making difficult to control the stability, morphology and polydispersity of the formed nanostructures.

The aim of the present work is to gain insights into the self-assembly of CFF in aqueous solution and verify the influence of peptide conformational changes at the interface of AuNPs. We explored the effects of nanoparticles on the peptide fibrillization process from both the perspectives of inducers and inhibitors of the CFF nucleation kinetics. We show that the latter dependent on the nanoparticle synthesis route, i.e., by using sodium borohydride ($NaBH_4$) as a reducing agent, or by using the peptide-catalyzed

redox technique for the *in situ* synthesis and stabilization of AuNPs under heating at 60ºC, as schematized in Figure 1.

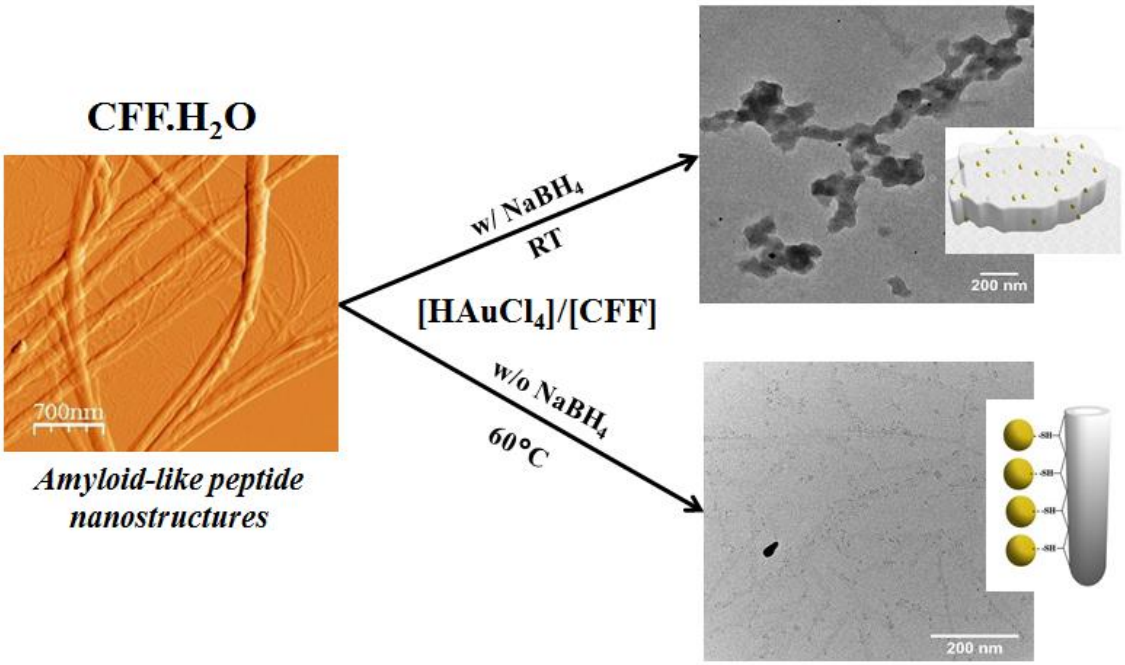

Figure 1. Schematic representation of the self-assembly process of CFF and AuNPs by using different experimental approaches.

2. RESULTS AND DISCUSSION

2.1. Spectroscopy and Morphological Studies of CFF

To evaluate the phenomena of self-organization and study the aggregation mechanism of CFF in aqueous media, seven CFF solutions in a range of 0.3-2.0 mmol·L^{-1} peptide concentrations were analyzed by steady-state fluorescence spectroscopy. The critical aggregation concentration (*cac*) was assessed by the normalized intensity of the phenylalanine fluorescence emission at λ= 289 nm.[40-43] In this way, the CFF *cac* (~0.8 mmol·L^{-1} at 25°C) was estimated from the crossover between linear fits corresponding to different emission regimes (Figure 2A). In aqueous solutions, CFF forms spontaneously a β-sheet conformation mainly stabilized by hydrogen bonding interaction (see Figure 2C). In addition, both electrostatic forces between the charged residues, and the hydrophobic

effect on the FF group contribute to the aggregation process, which is identified by the inflection point in the fluorescence intensity *vs.* peptide concentration curve. The latter indicates the transition from a monomer-like phase to the formation of an aggregate structure, characterized by a higher fluorescence due to water exclusion that cannot exert its quenching activity on the F fluorophore. This is confirmed by the slight blue shift of the F emission, due to the lower polarity of the water-excluded environment in the aggregate.

Moreover, we also observed that the CFF self-assembly can be influenced upon changing the pH of the solution. Although the CD spectra of Figure 2C are typical of an antiparallel β-sheet arrangement at all the pHs investigated (pH= 3.0, 7.0 and 10), their relative rotational strengths are not the same, suggesting that a different amount of β-sheet conformers populate the solutions at different pHs. As the pH decreases from 10 to 3.0, the ionization degree of CFF decreases, as can be seen in the titration curve (Figure 2B). Therefore, pH changes affect the interchain interactions of the aromatic peptide amphiphiles,[44] promoting CFF aggregation as Aβ-like structures.

CD spectra of CFF pre-assemblies (Figure 2C) in aqueous solution showed a negative peak at 190 nm, and two positive peaks at 200 nm and 217 nm corresponding to the π–π^* transition and n–π^* transition, respectively.[45] The shape of the CD curves was similar to that of β-turn peptides and π-stacked phenylalanine residues, which was characterized by a negative peak at 180–190 nm and two positive peaks at 200–205 nm and 220–230 nm.[41,46] It is inferred that at this concentration CFF achieves a higher level of organization that could be associated to the beginning of fibrillization in solution. This finding strongly suggests the possibility that this simple tripeptide can form amyloid-like fibers.

To investigate the morphology of the CFF aggregates, AFM images (Figure 2D) were acquired on dried samples obtained from a solution of peptide above the *cac*. The images show a network of entangled fibers at neutral pH with diameters ranging from 100 to 150 nm and lengths of up to a few micrometers, in coexistence with globular particles with a few tens of nanometers in diameter (see Figure 2D). The fibers are formed by smaller elliptical particles, which may be related to an Ostwald-like ripening process of coherent β-precipitates during the internal rearrangement of structures formed in a kinetically driven self-assembly process.[47] Spherical or granular aggregates were in some cases considered as precursors or nuclei for fibrillization as in the case of amyloid β-protein.[48]

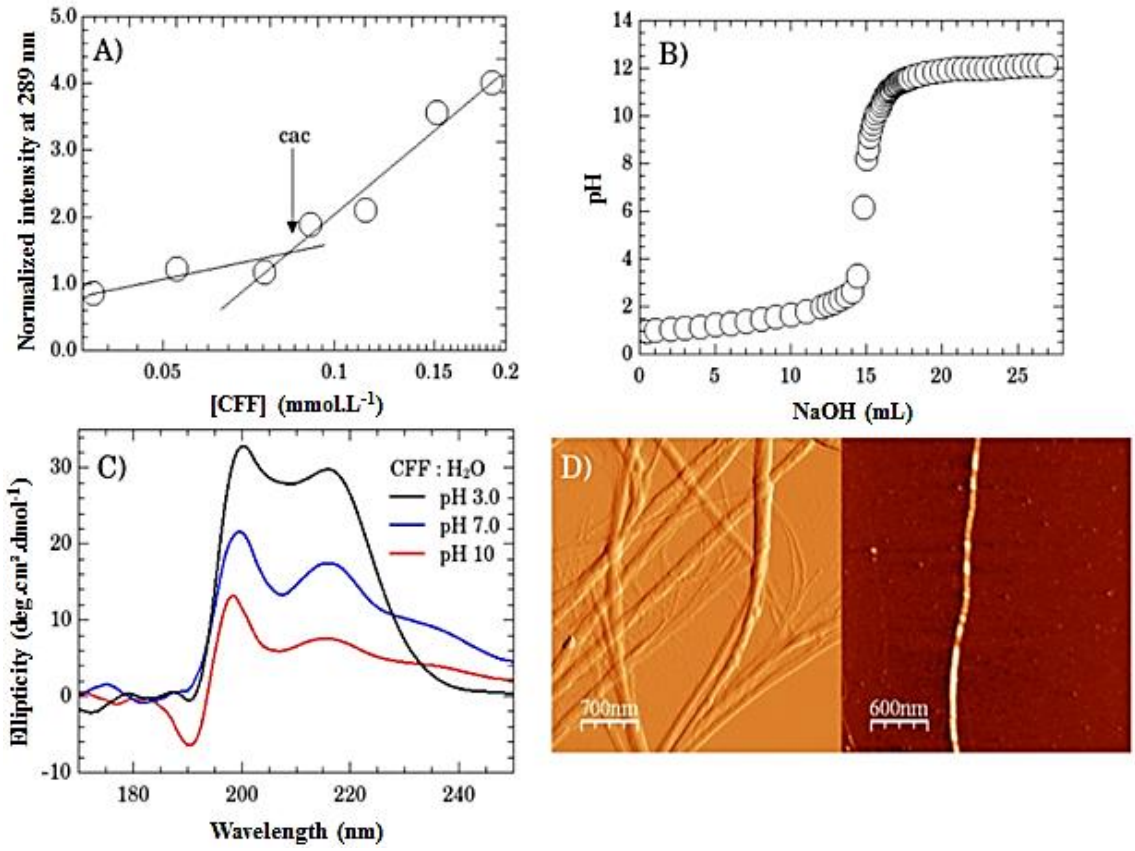

Figure 2. (A) Normalized fluorescence intensity at $\lambda_{emission}$= 289 nm *vs.* CFF molar concentration. The CFF *cac* is obtained at the crossing point of the linear interpolation of the fluorescence data in the two emission regimes ($\lambda_{excitation}$= 258 nm); (B) Titration curve of the CFF tripeptide at pH ranges of 1.0 to 12, by using a 0.1 mol·L^{-1} NaOH solution; (C) CD spectra of CFF solutions at

different pHs; (D) AFM images of a dried CFF solution ([CFF]= 8.4 x 10^{-4} mol·L^{-1}), showing the formation of fibers for concentrations above the *cac*, in different regions of the substrate.

Recently, Gazit and co-workers[47] studied the morphological transition of Boc-FF from a globular to a tubular phase, indicating that the transition from spheres to tubes is exothermic and that the concentration of monomers in equilibrium with the tubular phase is lower than that found in the case of monomers-spheres equilibrium. This finding suggests that the thermodynamic stability of the tubular phase is higher than that of the globular phase, and hence that the transition is governed by Ostwald´s rule of stages.[47]

2.2. Manipulating the assembly of cysteine-diphenylalanine in solution using AuNPs

AuNPs were synthesized *via* the $NaBH_4$ reduction of $HAuCl_4$ in the presence of the CFF. For the evaluation of the influence of the ratio [$HAuCl_4$]/[CFF] on the AuNPs size, three CFF concentrations near the *cac* of the peptide material (0.38, 0.75 and 1.1 mol·L^{-1}) were selected. These three concentrations correspond to [$HAuCl_4$]/[CFF] ratios of 2.7, 1.3, and 0.88, respectively. Optical absorption data (Figure 3A) show the typical gold plasmon resonance with maximum absorption wavelengths ranging from 526 to 549 nm, which is characteristic of spherical nanoparticles.[49] The observed blue-shift in plasmon resonance absorption band of the hybrids with respect to the CFF concentration is due to the reduction of the nanoparticle diameter from 55 to 20 nm. As it can be seen in Figure 3A, the intensity of the band decreases with the increase of the CFF concentration. Furthermore, the presence of the peptide in the AuNPs solution promotes the stabilization of the system (see Figure 3B).

The full width at half maximum (FWHM) of the plasmon band at 555 nm is shown in Figure 3C for all the samples investigated. The ~25 nm broadening of the plasmon band measured in the case of AuNPs obtained at [$HAuCl_4$]/[CFF]= 0.88 can be attributed to the

aggregation of nanoparticles embedded within the peptide matrix, which may occur when increasing the peptide content near a critical concentration ratio.

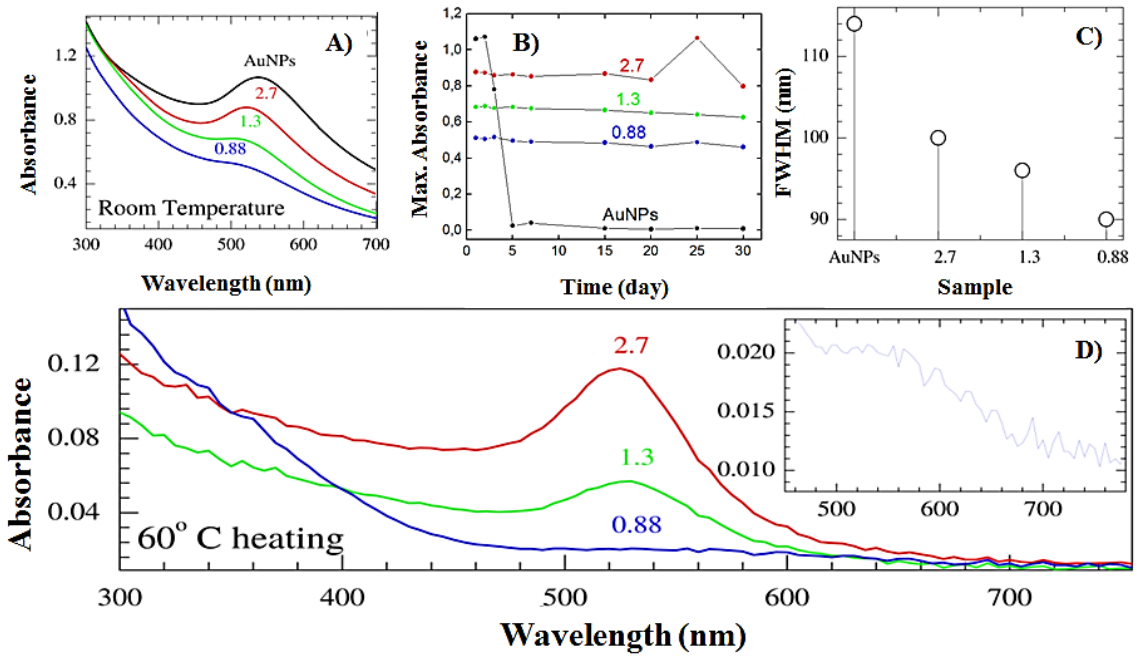

Figure 3. UV-Vis absorption spectrum of AuNPs synthesized at pH 7.0, in the absence (black) and in the presence of CFF, for the following $[HAuCl_4]/[CFF]$ ratios: 2.7 (red line); 1.3 (green line) and 0.88 (blue line) prepared at room temperature conditions with $NaBH_4$ (A) and under 60ºC heating (D). Time dependence of the shift of the Au SPR absorption band (B). Full width at half maximum (FWHM) of the SPR band at 555 nm for the samples presented in (A) is shown in (C). The inset of (D) shows a magnification of the SPR band for the 0.88 $[HAuCl_4]/[CFF]$ ratio under heating.

Figure 3D shows the UV-Vis spectra recorded for aqueous CFF-capped AuNPs dispersions at 60°C, considering the $[HAuCl_4]/[CFF]$ ratios: 2.7, 1.3 and 0.88. A very weak longitudinal plasmon resonance centered at *ca*. 520 nm is observed for low CFF concentration, that widens when the peptide proportion increases, indicating some aggregation of the AuNPs in the aqueous medium.

Direct evidence for aggregation of the CFF-coated AuNPs is provided by TEM studies which are presented in Figures 4 and 5. Initially, monodispersed solutions of AuNPs with

a mean size of about 3-9 nm were synthesized, obtaining a lower monodispersity upon decreasing the [$HAuCl_4$]/[CFF] ratio. In this case, the increasing peptide concentration onto the AuNP surfaces likely promoted the formation of small amorphous clusters. CFF adsorption on the AuNPs surfaces, decreases the CFF concentration in solution, thereby inhibiting the growth of fibrils or their elongation into massive aggregates. In other words, CFF monomers are strongly adsorbed onto the surface of thiol-AuNPs and conformational conversion of these surface-bound CFF to amyloid-like fibers would be hindered, resulting in retardation of Aβ aggregation.

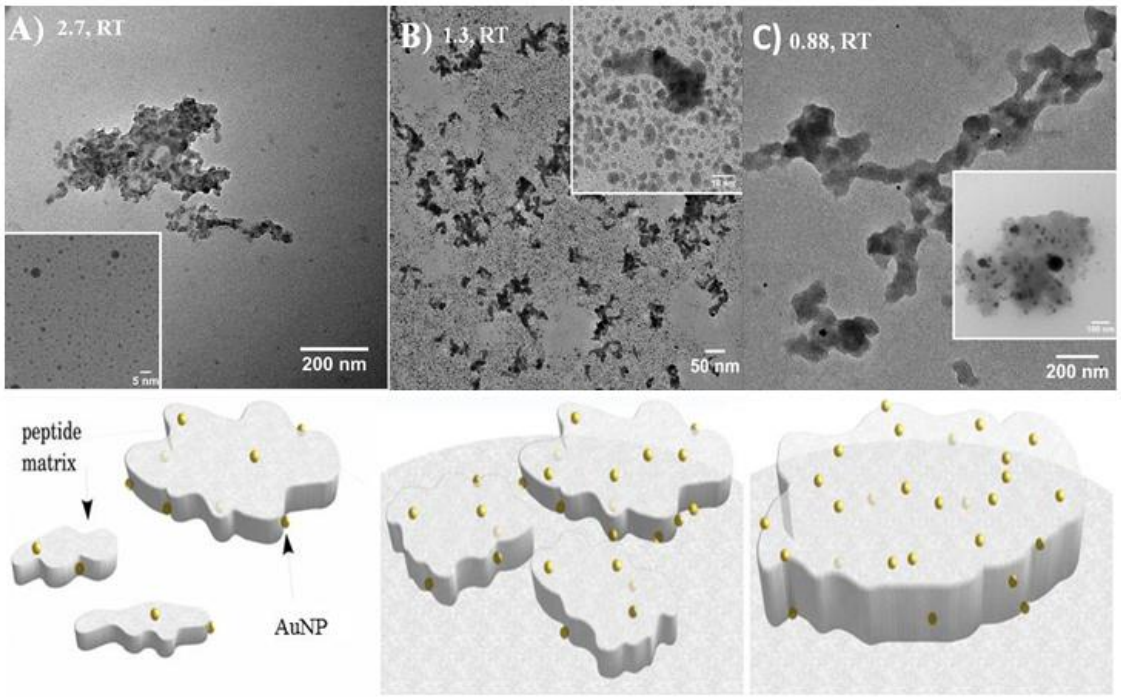

Figure 4. TEM images of [$HAuCl_4$]/[CFF] ratios: 2.7 (A); 1.3 (B); and 0.88 (C) prepared at room temperature conditions with $NaBH_4$.

On the other hand, there are various approaches to accelerate the spontaneous fibrillization of proteins, including agitation of the solution by shaking or stirring.[50] In this work, we found that increasing the time incubation of the CFF and $HAuCl_4$ reaction mixture at 60°C, but without the use of external reducing agents, induced fibrillization, depending on the ratio of the Au salt and capping agent (Figure 5). Reduction of the

chloroaurate ion by a cysteine moiety implies oxidation of the amino acid and self-reduction of the gold salt precursor.

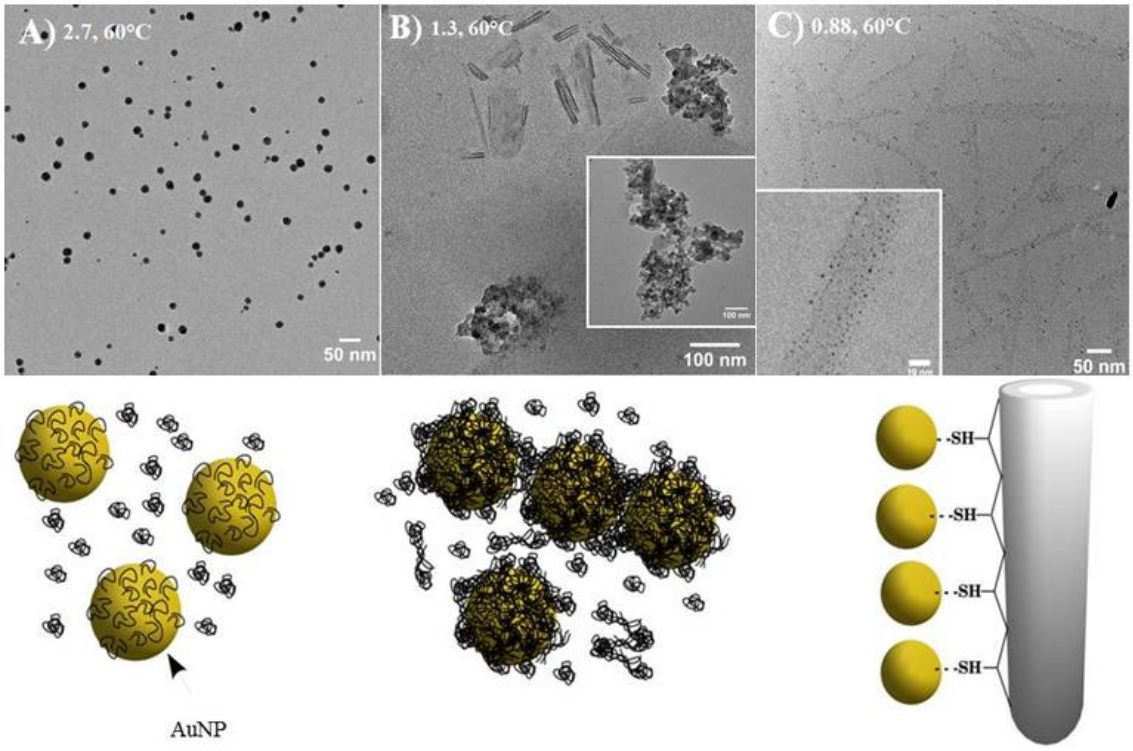

Figure 5. TEM images of AuNPs/CFF conjugates and schemes of the aggregation process for the [$HAuCl_4$]/ CFF] ratios: 2.7 (A); 1.3 (B); and 0.88 (C) prepared under heating at 60ºC.

The state of AuNPs aggregation associated with different CFF proportions is evidenced by the TEM results shown in Figures 4 and 5. In agreement with the UV-Vis spectroscopy results described above, AuNPs in the solutions prepared at higher [$HAuCl_4$]/[CFF] molar ratios are spherical and monodisperse with a particle size which may be varied within the range comprised between 10 and 15 nm (see Figure 5A). Increasing the amount of CFF in the system affected the stability of AuNPs in solution, promoting the formation of different polymorphs, including a mixture of small spheres, some amorphous aggregates and fibrils (Figure 5B). Some of the aggregation properties of the CFF peptides were thus transferred to the Au nanoparticles, and this may provide a strategy for the control of the AuNPs assembly.

At lower [$HAuCl_4$]/[CFF] ratios, i.e. with increasing the CFF concentration above the *cac*, a remarkably large fraction of peptide aggregates was present in the solution instead than on the nanoparticle surface. Thus, peptide aggregation as Aβ-like fibers predominantly occurs in solution as seen in AFM images (Figure 2D), instead than on the nanoparticle surface.

CFF forms fibrils the peptide layers of which could serve as a template for the formation of geometrically confined Au seeds (Figure 5C). Some smaller fibers had diameters of approximately 50 nm with lengths in the micrometer range. The observed morphology change proves that the addition of peptide-AuNPs facilitates the subsequent assembly of peptides into stable fibril aggregates by increasing the local concentration of those peptides. Nanoparticles may act like conventional catalysts by reducing the energy barrier to fibrillization increasing the population of prefibrillar aggregates.[19] A possible model illustrating both the formation of particle and fiber aggregates are schematized in Figures 4 and 5.

In order to evaluate the structure of self-assembled species in solution, SAXS experiments were performed firstly for the system containing just the peptide above the *cac* in water (Figure 6A) and different [$HAuCl_4$]/[CFF] ratios by using $NaBH_4$ as the reducing agent (Figure 6B), or by using the peptide-catalyzed redox technique for the *in situ* synthesis and stabilization of AuNPs under heating at 60ºC (Figure 6C). In order to get some information about the overall size of the CFF aggregates, two approaches were applied. By using the Indirect Fourier Transformation (IFT) approach, some initial indications for the shapes of the particles in solution were obtained. The results are shown as Supporting Information (SI). The results indicate that CFF in solution formed large polydisperse aggregates. When adding the nanoparticles, p(r) functions for different [$HAuCl_4$]/[CFF] ratios indicate the presence of large aggregates with a radius of ~2-3 nm.

For the heated system, the samples for 2.7 and 1.3 [$HAuCl_4$]/[CFF] ratios predominantly formed well-ordered agglomerates of globular shape. Interestingly, for the ratio 0.88 the IFT analysis provided results similar to the ones obtained at room temperature. As a further modeling procedure, an aggregated polydisperse spheres model with flexible parts was applied (see SI). As a result, we obtained a central radius of 6.0(5) nm with polydispersity of 3.0(2) nm and flexible parts with radius of gyration of 1.0(1) nm. These findings suggest an intrinsic flexibility on the aggregates. Even though alternative models may fit the scattering curve, this description provides some indications on the overall size of the formed aggregates. The results are summarized in Table 1.

For the hybrids, in all cases, colloidal solutions containing CFF-coated nanoparticles were stable for months with little evidence of precipitation. The scattering profiles can be divided in three distinct parts: at low q region (q < 0.3 nm^{-1}) the observed behavior is typical of the Guinier's region, which is used for the determination of the overall size of the particles. At q ~1.0 nm^{-1}, a subtle oscillation in the curve can be related to the overall size of AuNPs and its polydispersity. At high q region (q > 1.1 nm^{-1}) the curve has little information because this region, in our data, is dominated by the background and flexible parts signals.

As in the case of CFF in water, we used the model of aggregated polydisperse spheres with flexible parts to describe the SAXS data for the synthesis of AuNPs using $NaBH_4$ at room temperature (Figure 6B), for the three samples [$HAuCl_4$]/[CFF]= 2.7 (below *cac*), 1.3 (~ *cac*) and 0.88 (above *cac*).

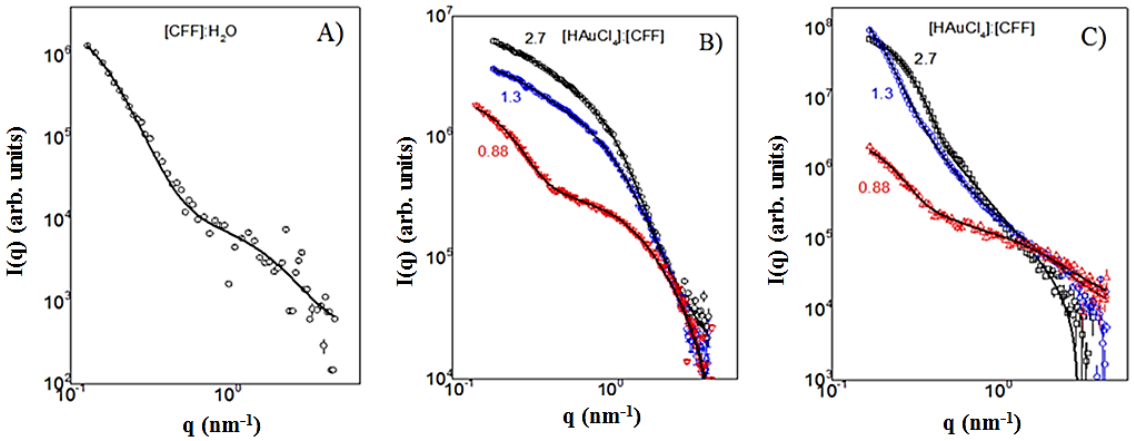

Figure 6. Small-angle scattering (SAXS) profiles from 7.5 x 10^{-3} mol·L^{-1} CFF in water (A) and for the following [$HAuCl_4$]/[CFF] ratios: 2.7 (black line); 1.3 (blue line) and 0.88 (red line) prepared at room temperature with $NaBH_4$ (B) and under heating (C).

As shown in Table 1, for the [$HAuCl_4$]/[CFF] samples obtained at room temperature using $NaBH_4$ the results indicate the presence of polydisperse spheres (3-5 nm), which aggregates on large domains with radius of gyration of ~7-8 nm. From the modeling procedure one obtained the presence of flexible domains with radius of gyration of ~1.5-3 nm. This result can be understood as an average contribution from all the flexible parts of the system. For the 0.88 ratio a significant increase on the scale factor of the aggregates (S_C^G) was found, which indicates an important increase on the aggregate fraction.

For the AuNPs obtained by synthesis under heating (Figure 6C), oscillations in the mid q region ($0.3 < q < 1.0$ nm^{-1}) were observed; this finding is associated with the presence of spherical particles with well-defined sizes, as imaged in the TEM experiments (Figure 5). As shown in Table 1, for the ratios 2.7 and 1.3 there is an enhanced formation of nanoparticles characterized by a very narrow distribution and without the presence of larger aggregates. For the ratio 0.88 there is a much weaker scattering intensity which indicates a lower concentration of particles. In this case the size of spherical particles decreases and larger aggregates can be readily observed. Above the

cac (ratio 0.88) somewhat similar SAXS results were obtained, indicating that concentration induced aggregates largely predominate.

Table 1. Summary of the model parameters obtained from the fitting procedure of SAXS data.

Sample	R [nm]	σ [nm]	Sc^G	R_G^{Agg} [nm]	Rg^{Gauss} [nm]
CFF	6.0(5)	3.0(2)	---	---	1.8(4)
$NaBH_4$ - $[HAuCl_4]$/[CFF]:					
2.7	2.9(5)	3.0(2)	1.4(4)	6.3(5)	3.0(5)
1.3	4.7(5)	3.0(2)	3.1(9)	7.3(3)	2.7(5)
0.88	5.1(15)	1.0(6)	17(9)	7.7(9)	1.5(6)
60°C - $[HAuCl_4]$/[CFF]:					
2.7	7.5(7)	1.9(5)	---	---	2.5(5)
1.3	11(2)	3.6(1)	---	---	2.0(5)
0.88	3.5(10)	1.0(6)	19(4)	8.7(2)	1.3(2)

Figure 7 presents dispersive Raman spectra for some representative samples (CFF·H_2O, AuNPs synthesis in $[HAuCl_4]$/[CFF] = 1.3 ratio at room temperature using $NaBH_4$ and at 60°C). The overall spectra are in agreement with those reported in the literature.[55] Figure 7 shows a very intense and narrow band at 1004 cm^{-1} and a band of lower intensity at 1600 cm^{-1}, related to the vibrations of the F aromatic ring.[51,52] The C-H vibrational modes are characterized by the band at 1450 cm^{-1}. The vibrational bands at 292, 387, and 735 cm^{-1} are present only in the CFF·H_2O sample. From DFT vibrational modes calculation on *L*-Cysteine, we attributed these bands to S···O^{donor} stretching (292 cm^{-1}), skeletal NH_3-C-S-O vibration (387 cm^{-1}), and N-C-S thiocyante stretching (735 cm^{-1}). Thus, their absence on AuNPs samples is an indirect confirmation of the gold coordination to the cysteine side chains from the fibers.

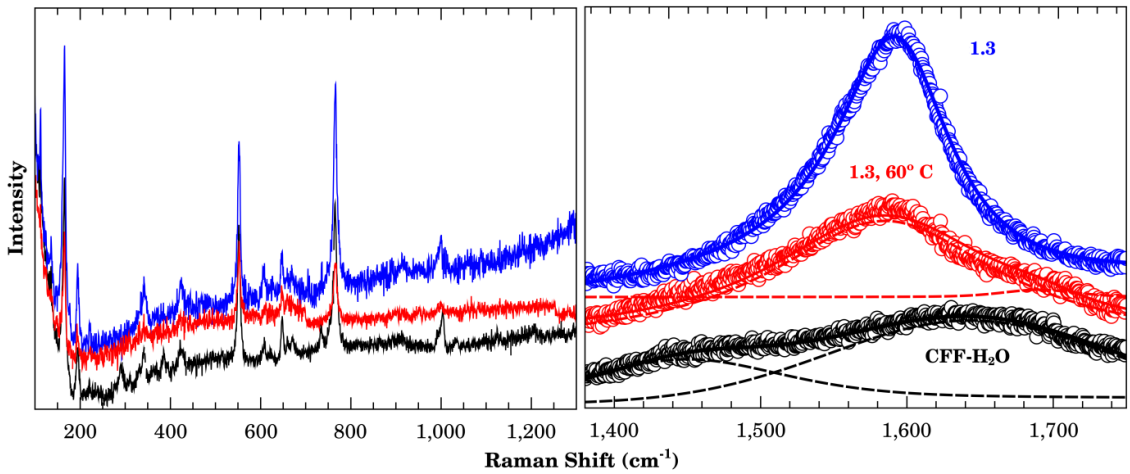

Figure 7. Dispersive Raman spectra for solutions with 7.5 x 10^{-4} mol·L^{-1} of CFF in water (black line) and considering the synthesis of AuNPs using $NaBH_4$ (blue line) and under heating (red line).

The peptide fibers hosting AuNPs presented an asymmetric F band peaked at 1600 cm^{-1}. Charge transfer across the aromatic ring could give rise to interference between phonon and electron wavefunctions (Fano resonance), which manifests itself as an asymmetric lineshape and peak shifting according to Equation 1:

$$I = I_0 \frac{[1 + (\omega - \omega_0)/q\,\Gamma]^2}{1 + [(\omega - \omega_0)/\Gamma]^2} \qquad (eq.1)$$

where q, Γ, and ω_0 are the asymmetry parameter, linewidth, and phonon frequency, respectively.[53] The product $q\Gamma \propto \langle e|V|ph\rangle$, accounts for the electron-phonon constant coupling. The lineshapes for [$HAuCl_4$]/[CFF] = 1.3 at room temperature and under 60ºC heating samples are shown in Figure 7. The values found for $q\Gamma$ were -480 cm^{-1} and -3900 cm^{-1}, respectively. The one order of magnitude larger electron-phonon constant coupling for the sample produced under heating is related to the low dimensionality of this sample compared to the others. It is interesting to mention that the Fano resonance is absent in others Raman bands. We argue that this fact is an evidence for F ring charge

localization. The negative values of qΓ indicates that the carriers are electrons (*n*-type charge localization).

The insertion of AuNPs at the surface of CFF nanostructures can promote the formation of negative charges (-31 mV, as obtained by Zeta potential measurements) that can be excited using a 532 nm laser radiation. This can promote electron transfer from the AuNPs to the CFF surface, creating an n-type semiconductor, and causing a peak shift of the F absorption band. Comparing the methodologies for the nucleation of AuNPs, the intensity of the band is higher for the $NaBH_4$ reduction method than for heating at 60°C sample; this can be indicative of the stronger n-doping of CFF applying the former procedure.[54,55]

In order to monitor the excimer formation process,[56] the samples were excited at 330 nm to reveal the characteristic emission band of the formed aggregates (λ_{em}=423 nm). The emission band was measured after a 24 hours preincubation of CFF·H_2O stock solution in the presence and absence of gold nanoparticles under different reaction conditions. As shown in Figure 8, the tripeptide shows two bands at 370 and 420 nm, which can be associated with the formation of globules (micellar aggregates) and fibers, respectively.[56] The control (CFF·H_2O) presents a very high intensity emission typical of micellar aggregates, indicating that in this system spherical aggregates predominate. For the sample under heating, both aggregate bands are present, but the intensity of the excimer band is definitely higher, signalling the formation of more ordered, crystalline structures, favoring the fibrillization of the peptide material. The hybrid sample obtained by $NaBH_4$ reduction presents almost the same contribution for both the aggregate types, suggesting a slower kinetics for the formation of crystalline aggregates, making the fibrillization process more difficult, in fair agreement with the TEM and SAXS results.

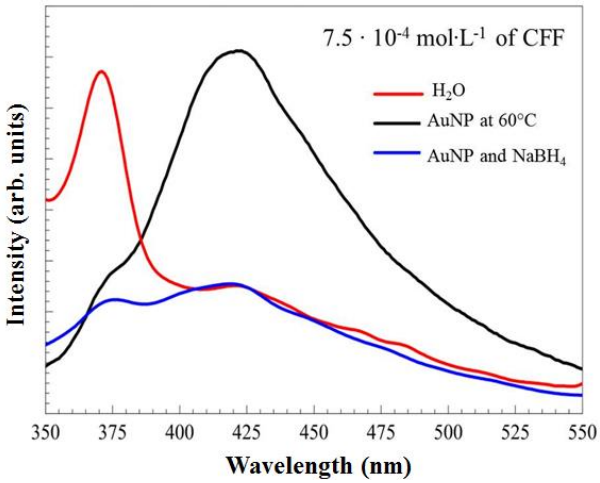

Figure 8. Fluorescence spectra for solutions with 7.5 x 10^{-4} mol·L^{-1} of CFF in water (red line) and with AuNPs using $NaBH_4$ (blue line) and under heating (black line); $\lambda_{excitation}$ = 330 nm.

Therefore, we provided a single-step process that allows for the simultaneous formation of highly ordered nanostructures, where the size of peptide-gold nanoparticle hybrid systems could be controlled by using different $[HAuCl_4]$/[CFF] ratios, reducing agents, and temperature-dependent reaction conditions. This method, which combines peptide-based supramolecular structures with desirable functional inorganic materials, may provide a novel approach for "bottom-up" fabrication of hierarchical structures with unique physical, chemical, and biological properties.

3. CONCLUSIONS

In summary, we have demonstrated the fabrication of hybrid nanostructures containing CFF and gold nanoparticles in water. Furthermore, the size of AuNPs in the self-assembly of an amyloid-like peptide can be tuned by adjusting the $[HAuCl_4]$/[CFF] proportion, temperature of the reaction, and reducing agent. The fibrillization process was faster for the CFF-AuNP conjugates under heating, promoting the formation of crystalline aggregates. However, amorphous structures were obtained in aqueous solution at room temperature by using $NaBH_4$ as the reducing agent. Another parameter to be

considered is the peptide concentration. Below the *cac*, the system gave rise to the formation of polydisperse globular nanoparticles; while above the *cac*, the formation of fibrillar compounds with diameters in the order of ~50 nm takes place. In both cases, the nanoparticles are distributed inside and on the surface of the peptide nanostructures, indicating that the simultaneous self-assembly of the peptides and nucleation of the gold salt via specific interaction, propagate the molecular-scale ordering to the nanoscale morphology. For both synthetic methods, it was verified that the systems self-organize as polydisperse globules, with the presence of flexible parts. The insertion of AuNPs at the surface of CFF nanostructures can promote electron transfer from the metallic nanoparticles to the CFF surface, creating an n-type semiconductor. The method developed here may be useful to produce various multifunctional hybrid nanostructures that may find potential applications in nanotechnology and biomedical science.

SUPPORTING INFORMATION SUMMARY

The experimental procedures and additional characterization data are provided in supporting information.

CONFLICT OF INTEREST

The authors declare no competing financial interests.

ACKNOWLEDGEMENTS

This work was supported by FAPESP (grant nos. 2015/24018-1, 2017/02317-2 and 2016/24409-3) and CNPq (grant no. 302923/2015-2). INCT in Bioanalytics (FAPESP grant no. 2014/50867-3 and CNPq grant no. 465389/2014-7) is kindly acknowledged for the grants. J.N.B.D.P. acknowledges FAPESP (project number 2015/20446-9) for a

doctoral fellowship. This project has also received funding from the European Union's Horizon 2020 research and innovation programme under the Marie Skłodowska-Curie grant agreement No 690901. The staff at LNNano and LNLS are kindly recognized for invaluable help and access to AFM, TEM, SAXS facilities, respectivelly. The authors are grateful to the Multiuser Central Facilities (UFABC), Nanomedicine Research Strategic Unit (NANOMED) at UFABC and Instituto de Física – USP for the experimental support. C.L.P.O. is supported by the National Council for Scientific and Technological Development, the Coordination for the Improvement of Higher Education Personnel (CAPES), the National Institute of Science and Technology Complex Fluids (INCT-FCx), and the São Paulo Research Foundation.

KEYWORDS: Amyloids, Crystal nucleation and growth, Gold nanoparticles, n-type semiconductor, Peptide assemblies.

REFERENCES

[1] S. Brown, M. Sarikaya, E. Johnson, *J. Mol. Biol.* **2000**, *299*, 725-735.

[2] R. R. Naik, S. J. Stringer, G. Agarwal, S. E. Jones, M. O. Stone, *Nat. Mater.* **2002**, *1*, 169-172.

[3] J. M. Slocik, M. O. Stone, R. R. Naik, *Small* **2005**, *1*, 1048-1052.

[4] J. Conde, A. Ambrosone, V. Sanz, Y. Hernandez, V. Marchesano, F. Tian, H. Child, C. C. Berry, M. R. Ibarra, P. V. Baptista, C. Tortiglione, J. M. de la Fuente, *ACS Nano.* **2012**, *6*, 8316-8324.

[5] I. W. Hamley, *Chem. Rev.* **2012**, *112*, 5147-5192.

[6] J. Geng, K. Qu, J. Ren, X. Qu, *Mol. Biosyst.* **2010**, *6*, 2389-2391.

[7] G. Wei, Z. Su, N. P. Reynolds, P. Arosio, I. W. Hamley, E. Gazit, R. Mezzenga, *Chem. Soc. Rev.* **2017**, *46*, 4661-4708.

[8] T. Takahashi, H. Mihara, *Acc.Chem.Res.* **2008**, *41*, 1309-1318.

[9] Z. Wang, L. Ma, *Coord. Chem. Rev.* **2009**, *253*, 1607-1618.

[10] A. Gilam, J. Conde, D. Weissglas-Volkov, N. Oliva, E. Friedman, N. Artzi, N. Shomron, *Nat. Commun*. **2016**, *7*, 12868-12882.

[11] J. Conde, F. Tian, Y. Hernández, C. Bao, D. Cui, K. Janssen, M. R. Ibarra, P. V. Baptista, T. Stoeger, J. M. de la Fuente, *Biomaterials* **2013**, *34*, 7744-7753.

[12] M. McCully, M. S. Navarro, M. Teixidó, E. Giralt, *Curr. Pharm. Des*. **2017**, *23*, 1-11.

[13] A. A. Shemetov, I. Nabiev, A. Sukhanova, *ACS Nano* **2012**, *6*, 4585-4602.

[14] K. A. Moore, K. M. Pate, D. D. Soto-Ortega, S. Lohse, N. van der Munnik,; M. Lim, K. S. Jackson, V. D. Lyles, L. Jones, N. Glassgow, V. M. Napumecheno, S. Mobley, M. J. Uline, R. Mahtab, C. J. Murphy, M. A. Moss, *J. Biol. Eng.* **2017**, *11*, 5, 1-11.

[15] A. Gladytz, M. Wagner, T. Häupl, C. Elsner, B. Abel, *Part. Part. Syst. Charact.* **2015**, *32*, 573-582.

[16] A. Parnsubsakul, S. Oaew, W. Surareungchai, *Nanoscale* 2018, 1-11.

[17] T. Yang, X. Zhang, J. Yang, Y. Wang, M. Chen, *Talanta* **2018**, *177*, 212-216.

[18] X. Lu, D. Jiang, J. Yan, Z. Ma, X. Luo, T. Wei, Y. Xu, Q. He, *Talanta* **2018**, *179*, 646-651.

[19] M. Zaman, E. Ahmad, A. Qadeer, G. Rabbani, R. H. Khan, *Int. J. Nanomed.* **2014**, *9*, 899-912.

[20] Y. D. Álvarez, J. A. Fauerbach, J. V. Pellegrotti, T. M. Jovin, E. A. Jares-Erijman, F. D. Stefani, *Nano Lett.* **2013**, *13*, 6156-6163.

[21] D. Zhang, O. Neumann, H. Wang, V. M. Yuwono, A. Barhoumi, M. Perham, J. D. Hartgerink, P. Wittung-Stafshede, N. J. Halas, *Nano Lett.* **2009**, *9*, 666-671.

[22] Y. Xia, P. Yang, Y. Sun, Y. Wu, B. Mayers, B. Gates, Y. Yin, F. Kim, H. Yan, *Adv. Mater.* **2003**, *15*, 353-389.

[23] E. Kasotakis, E. Mossou, L. Adler-Abramovich, E. P. Mitchell, V. T. Forsyth, E. Gazit, A. Mitraki, *Pept. Sci.* **2009**, *92*, 164-172.

[24] T. Scheibel, R. Parthasarathy, G. Sawicki, X.-M. Lin, H. Jaeger, S. L. Lindquist, *Proc. Natl. Acad. Sci.* **2003**, *100*, 4527-4532.

[25] C.-L. Chen, N. L. Rosi, *Angew. Chem. Int. Ed.* **2010**, *49*, 1924-1942.

[26] M. Reches, E. Gazit, *Science* **2003**, *300*, 625-627.

[27] L. Adler-Abramovich, M. Reches, V. L. Sedman, S. Allen, S. J. B. Tendler, E. Gazit, *Langmuir* **2006**, *22*, 1313-1320.

[28] X. Yan, P. Zhu, J. Li, *Chem. Soc. Rev.* **2010**, *39*, 1877-1890.

[29] T. O. Mason, D. Y. Chirgadze, A. Levin, L. Adler-Abramovich, E. Gazit, T. P. J. Knowles, A. K. Buell, *ACS Nano* **2014**, *8*, 1243-1253.

[30] J. Wang, K. Liu, L. Yan, A. Wang, S. Bai, X. Yan, *ACS Nano* **2016**, *10*, 2138-2143.

[31] T. Andrade-Filho, T. C. Martins, F. F. Ferreira, W. A. Alves, A. R. Rocha, *Theor. Chem. Acc.* **2016**, *135*, 185-193.

[32] M. I. Souza, E. R. Silva, Y. M. Jaques, F. F. Ferreira, E. E. Fileti, W. A. Alves, *J. Pept. Sci.* **2014**, *20*, 554-562.

[33] P. Tamamis, L. Adler-Abramovich, M. Reches, K. Marshall, P. Sikorski, L. Serpell, E. Gazit, G. Archontis, *Biophys. J.* **2009**, *96*, 5020-5029.

[34] T. H. Han, T. Ok, J. Kim, D. O. Shin, H. Ihee, H.-S. Lee, S. O. Kim, *Small* **2010**, *6*, 945-951.

[35] C. Guo, Z. A. Arnon, R. Qi, Q. Zhang, L. Adler-Abramovich, E. Gazit, G. Wei, *ACS Nano* **2016**, *10*, 8316-8324.

[36] E. Mayans, J. Casanovas, A. M. Gil, A. I. Jiménez, C. Cativiela, J. Puiggalí, C. Alemán, *Langmuir* **2017**, *33*, 4036-4048.

[37] L. Adler-Abramovich, E. Gazit, *Chem. Soc. Rev.* **2014**, *43*, 6881-6893.

[38] M. Reches, E. Gazit, *Nano Lett.* **2004**, *4*, 581-585.

[39] B. B. Gerbelli, E. R. Silva, B. M. Soares, W. A. Alves, E. A. Oliveira, *Langmuir* **2018**, *34*, 2171-2179.

[40] K. E. Marshall, K. L. Morris, D. Charlton, N. O'Reilly, L. Lewis, H. Walden, L. C. Serpell, *Biochemistry* **2011**, *50*, 2061-2071.

[41] M. J. Krysmann, V. Castelletto, A. Kelarakis, I. W. Hamley, R. A. Hule, D. J. Pochan, *Biochemistry* **2008**, *47*, 4597-4605.

[42] R. C. G. Creasey, Y. Shingaya, T. Nakayama, *Mater. Chem. Phys.* **2015**, *158*, 52-59.

[43] V. Castelletto, P. Ryumin, R. Cramer, I. W. Hamley, M. Taylor, D. Allsop, M. Reza, J. Ruokolainen, T. Arnold, D. Hermida-Merino, C. I. Garcia, M. C. Leal, E. Castaño, *Sci. Rep.* **2017**, *7*, 43637-43649.

[44] C. Tang, A. M. Smith, R. F. Collins, R. V. Ulijn, A. Saiani, *Langmuir* **2009**, *25*, 9447-9453.

[45] X. Yan, Y. Cui, Q. He, K. Wang, J. Li, *Chem. Mater.* **2008**, *20*, 1522-1526.

[46] M. J. Krysmann, V. Castelletto, I. W. Hamley, *Soft Matter* **2007**, *3*, 1401-1406.

[47] A. Levin, T. O. Mason, L. Adler-Abramovich, A. K. Buell, G. Meisl, C. Galvagnion, Y. Bram, S. A. Stratford, C. M. Dobson, T. P. J. Knowles, E. Gazit, *Nat. Commun.* **2014**, *5*, 5219-5227.

[48] L. N. Arnaudov, R. de Vries, *Biophys. J.* **2005**, *88*, 515-526.

[49] P. K. Jain, X. Huang, I. H. El-Sayed, M. A. El-Sayed, *Plasmonics* **2007**, *2*, 107-118.

[50] M. Adachi, M. So, K. Sakurai, J. Kardos, Y. Goto, *J. Biol. Chem.* **2015**, *290*, 2395-2404.

[51] C. Blum, L. Opilik, J. M. Atkin, K. Braun, S. B. Kämmer, V. Kravtsov, N. Kumar, S. Lemeshko, J.-F. Li, K. Luszcz, T. Maleki, A. J. Meixner, S. Minne, M. B. Raschke, B. Ren, J. Rogalski, D. Roy, B. Stephanidis, X. Wang, D. Zhang, J.-H. Zhong, R. Zenobi, *J. Raman. Spectrosc.* **2014**, *45*, 22-31.

[52] D. Kurouski, R. P. Van Duyne, I. K. Lednev, *Analyst* **2015**, *140*, 4967-4980.

[53] M. Cardona, G. Güntherodt, In *Light Scattering in Solids IV: Electronics Scattering, Spin Effects, SERS, and Morphic Effects*, Springer-Verlag, Berlin, Vol. *54*, **1984**, p. 544.

[54] S. Huh, J. Park, K. S. Kim, B. H. Hong, S. B. Kim, *ACS Nano* **2011**, *5*, 3639-3644.

[55] X. Zheng, W. Chen, G. Wang, Y. Yu, S. Qin, J. Fang, F. Wang, X.-A. Zhang, *AIP Adv.* **2015**, *5*, 057133.

[56] A. R. Hirst, S. Roy, M. Arora, A. K. Das, N. Hodson, P. Murray, S. Marshall, N. Javid, J. Sefcik, J. Boekhoven, J. H. van Esch, S. Santabarbara, N. T. Hunt, R. V. Ulijn, *Nat. Chem.* **2010**, *2*, 1089-1094.

[57] L. A. Carpino, G. Y. Han, *J. Am. Chem. Soc.* **1970**, *92*, 5748-5749.

[58] E. Kaiser, R. L. Colescott, C. D. Bossinger, P. I. Cook, *Anal. Biochem.* **1970**, *34*, 595-598.

[59] A. P. Hammersley, S. O. Svensson, M. Hanfland, A. N. Fitch, D. Hausermann, *High Press. Res.* **1996**, *14*, 235-248.

[60] L. P. Cavalcanti, I. L. Torriani, T. S. Plivelic, C. L. P. Oliveira, G. Kellermann, *Rev. Sci. Instrum.* **2004**, *75*, 4541-4546.

[61] O. Glatter, *J. Appl. Cryst.* **1977**, *10*, 415-421.

[62] C. L. P. Oliveira, M. A. Behrens, J. S. Pedersen, *J. Mol. Biol.* **2009**, *387*, 147-161.

[63] C. L. P. Oliveira, D. A. Chandrasekaran. In *Current Trends in X-Ray Crystallography*, InTech, **2011**, p. 367.

[64] C. L. P. Oliveira, A. M. Monteiro, A. M. Figueiredo Neto, *Braz. J. Phys.* **2014**, *44*, 753-764.

[65] C. L. P. Oliveira, P. R. Santos, A. M. Monteiro, A. M. Figueiredo Neto, *Biophys. J.* **2014**, *106*, 2595-2605.

TABLE OF CONTENTS ENTRY

We show that the gold nanoparticles may both affect the structure of a short amyloid-like peptide in aqueous medium and promote electron transfer from the metallic nanoparticles to the peptide surface, creating an *n*-type semiconductor.